Journal of Hydrology 401 (2011) 203–220

Contents lists available at ScienceDirect

Journal of Hydrology

journal homepage: www.elsevier.com/locate/jhydrol

Influence of atmospheric correction and number of sampling points on the accuracy of water clarity assessment using remote sensing application

Nutchanart Sriwongsitanon [a,*], Kritsanat Surakit [b], Sansarith Thianpopirug [a]

[a] Department of Water Resources Engineering, Faculty of Engineering, Kasetsart University, Bangkok 10900, Thailand
[b] Department of Civil Engineering, Faculty of Engineering, Mahidol University, Nakhonpathom 73170, Thailand

ARTICLE INFO

Article history:
Received 2 October 2009
Received in revised form 9 December 2010
Accepted 17 February 2011
Available online 24 February 2011

This manuscript was handled by L. Charlet, Editor-in-Chief, with the assistance of Jose D. Salas, Associate Editor

Keywords:
Atmospheric correction
Sampling point
Water clarity
Landsat
Secchi disk transparency
Suspended sediment

SUMMARY

The main objectives of the research described in this paper are to assess the influence of atmospheric correction and the number of sampling points on the accuracy of lake water clarity using remote sensing. For this purpose field experiments were carried out at Bung Boraphet – the largest fresh water lake in Central Thailand. Two clarity parameters, secchi disk transparency (SDT), at 80 locations for three events on April 15th 2008 and March 24th and 31st 2009, and suspended sediment concentration (SSC) for the last two events were collected. These field data were collected nearly contemporaneous or contemporaneous to three Landsat 5 TM images, which were acquired on April 13th 2008 and March 24th and 31st 2009, respectively. Digital numbers of the Thematic Mapper (TM) image bands were transformed to at-sensor radiance by a radiometric correction process and then atmospheric correction was made using the Second Simulation of Satellite Signal in the Solar Spectrum (6S) code to acquire the surface reflectance. Linear regression equations between the log-transformed of clarity parameters and surface reflectance of each band and their band ratios at the same pixels were then determined. The band combinations TM1/TM3 and TM1 to estimate ln(SDT), and TM3/TM1 and TM1 to determine ln(SSC) for all satellite images were selected. These equations were later used to estimate the SDT and SSC values distributed across the whole lake. The results showed that lake wide average values of SDT for the three images are approximately 37, 97 and 81 cm, respectively, while the values of SSC for the second and third images are around 11 and 13 mg/l, respectively. The application of atmospheric correction to the TM data has proved to have the effect on the average values of SDT and SSC, and especially on their maximum and minimum values. Finally, it is possible to reduce the ground observation data of SDT and SSC substantially and still obtain reliable empirical relationships for the estimation of lake wide SDT and SSC values from TM data within the lake.

1. Introduction

Lakes are valuable freshwater resources that can be used for various purposes such as for drinking water, agriculture, fishing, recreation and tourism (Oyama et al., 2009). Unfortunately, water quality in a number of lakes around the world is becoming degraded by a variety of anthropogenic causes.

Monitoring water quality is a vital aspect of lake management to determine its suitability for human uses and to inform on the need to take corrective actions in the event that water is not fit for use. Conventional field methods for lake water sampling are time consuming and expensive, however satellite imagery is another source of information with great potential to be used for assessment of lake water quality. Processing and interpretation of satellite imagery are now becoming relatively inexpensive and easy to perform with today's powerful desktop computers and sophisticated software.

However, empirical relationships between satellite data and contemporaneous ground observations are always necessary for evaluating the spatial variation of water quality variables within the lake. Among several satellite systems that have been used for water quality assessment, the Landsat system is particularly useful for assessment of inland lakes (Kloiber et al., 2002). Several investigations have developed reliable empirical relationships between Thematic Mapper (TM) data and ground observations of water quality characteristics (Brown et al., 1977; Giardino et al., 2001; Jie et al., 2006; Kloiber, et al., 2002; Lathrop and Lillesand, 1986; Olmanson et al., 2008; Ostlund et al., 2001). Regardless of the method they are constructed, the empirical and semi-empirical relationships are generally site specific (Liu et al., 2003). Up to

* Corresponding author. Address: Department of Water Resources Engineering, Faculty of Engineering, Kasetsart University, 50 Paholyothin Rd., Ladyao, Jatujak, Bangkok 10900, Thailand. Tel./fax: +66 2 5791567.
E-mail addresses: fengnns@ku.ac.th (N. Sriwongsitanon), s_kritsanat@yahoo.com (K. Surakit), g5185060@ku.ac.th (S. Thianpopirug).

0022-1694/$ - see front matter © 2011 Elsevier B.V. All rights reserved.
doi:10.1016/j.jhydrol.2011.02.023

the present efforts to produce standard prediction equations for water quality parameters applicable to images collected on different dates at the same location have not been successful. Use of a consistent equation form to relate ground observations and satellite data is however preferable because it allows for easier comparison of the results from different images (Kloiber et al., 2002). However the relationships will vary from one event to another because the relationships are empirical by nature.

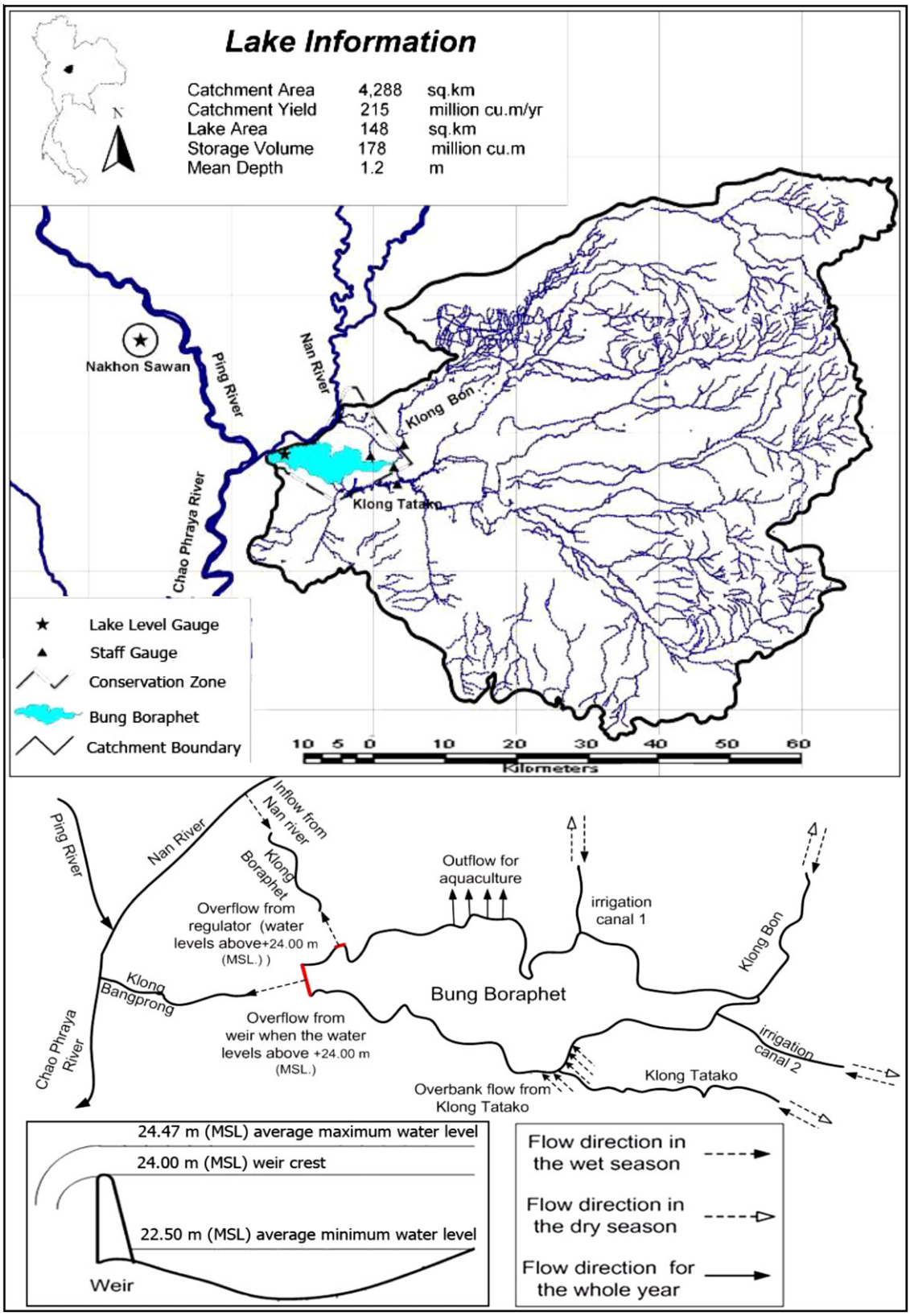

Fig. 1. Bung Boraphet and its drainage area.

This study was conducted at Bung Boraphet to derive empirical relationships for estimation of secchi disk transparency (SDT) and suspended sediment concentration (SSC) from three Landsat 5 TM images and in situ sampled data. Three TM images covering Bung Boraphet were acquired on April 13th 2008 and March 24th and 31st 2009. SDT ground observation data were collected on April 15th 2008 and March 24th and 31st 2009, while SSC data were collected only on the last two days. Ground observation data for the first event is nearly contemporaneous to the satellite image, while the last two events are contemporaneous to the images. SDT was chosen because it is used frequently to identify trends in lake conditions due to its simplicity and relatively low cost (Heiskary et al., 1994). SSC was selected because it reflects the physical and chemical property of water and relates to the total primary productivity of the lake (Jie et al., 2006).

Pattiaratchi et al. (1994) found that log-transformed SDT data produced strong correlations to TM data and follow a normal distribution. Klemas et al. (1974) found that a log-transformed SSC relationship to the Landsat Multispectral Scanner (MSS) data is better than a relationship in the original SSC domain. Therefore, log-transformed SDT and SSC versus untransformed TM data were therefore used in deriving the regression equations.

Prior to deriving these relationships, geometric, radiometric and atmospheric corrections were applied to the Landsat 5 TM images. The atmospheric correction was performed using 6S (Second Simulation of the Satellite Signal in the Solar Spectrum), which is a physically-based atmospheric correction model. Several researchers have found that 6S is an effective model for correcting satellite images affected by atmospheric factors. For example, Stroeve et al. (1997) and Zhao et al. (2001) found significant improvements in albedo after atmospheric corrections were applied on their AVHRR and Landsat TM data. Zhao et al. (2001) claimed that there was around 6% improvement in surface albedo after the correction. Also Sharma et al. (2009) concluded that corrected reflectance data better separated ground features such as water bodies and crop fields compared to uncorrected data.

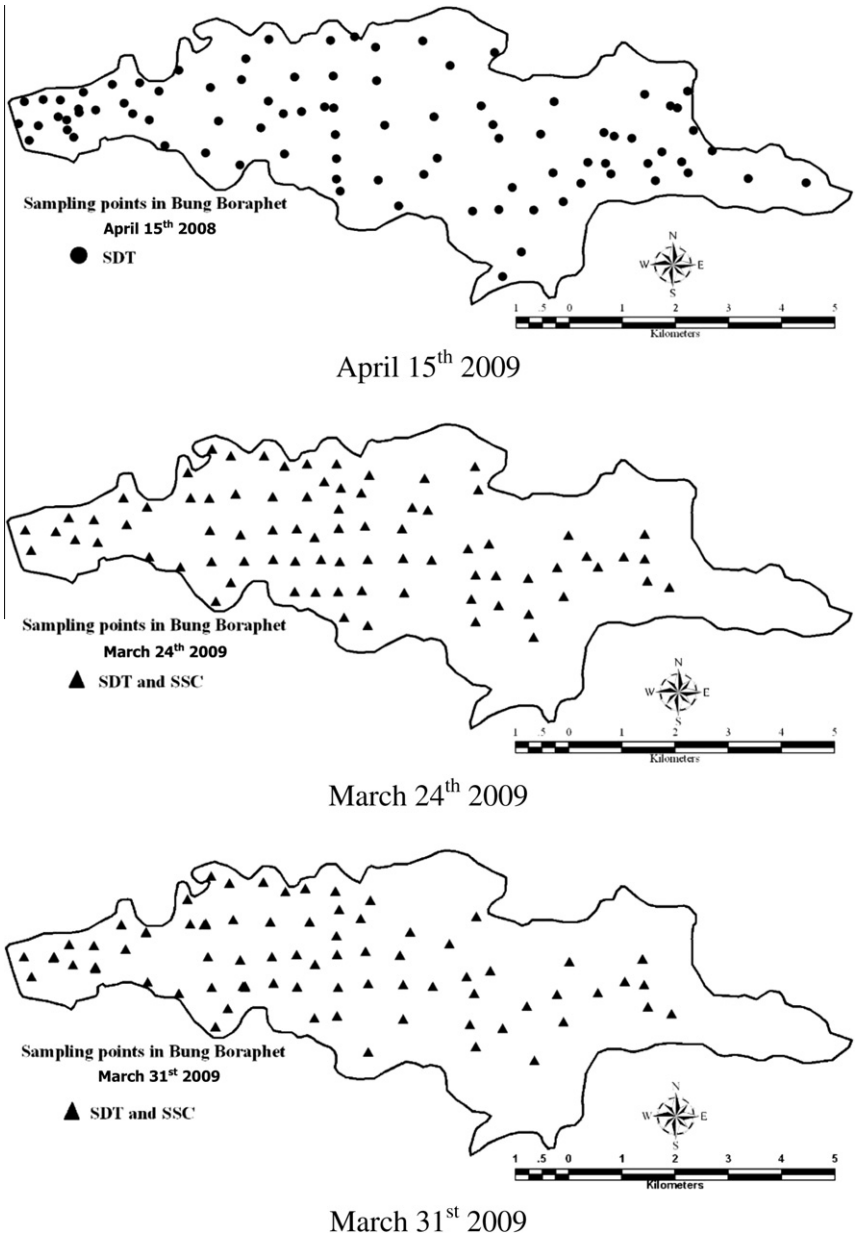

Fig. 2. Sampling points in Bung Boraphet of each ground observation.

This study has two main objectives. Firstly, to test whether atmospheric correction is needed for improving the reliability of the estimated values of SDT and SSC distributed within the lake. The estimated values of SDT and SSC for all pixels of each image, with and without atmospheric correction, were compared for their differences. Secondly, to investigate the minimum number of ground sampling points of SDT and SSC necessary for constructing reliable empirical relationships. To do this, subsets of points were chosen randomly from the overall set of sampling points and empirical relationships between SDT and SSC values versus TM image data were prepared. Then SDT and SSC values calculated using the subsets of sampling points were compared to values determined using the whole set to see whether it is possible to reduce the numbers of ground observation points but still provide reliable relationships.

2. Study area

Bung Boraphet is situated between latitude 15°40′ N (1732407N) and 15°45′ N (1741767N) and longitude 100°10′ E (625350 E) and 100°23′ E (648260 E) near the Nakhonsawan province on the floodplain of Thailand's largest river – the Chao Phraya. This location is near the confluence of the Ping and Nan rivers at the head of the Chao Phraya (Fig. 1). The entire floodplain including the lake and surrounding wetland can be submerged in large flood events on the Chao Phraya River. The lake receives water from a drainage area of 4288 km^2.

Two main streams, Klong Tatako and Klong Bon, which cover around 73% and 26% of the total catchment area, respectively, are connected to the lake. The surrounding catchment is extremely flat so these klongs perform numerous water transfer functions, particularly: (a) transmitting runoff from the catchment to the lake during high rainfall events and (b) transmitting irrigation water from the lake to upstream farms.

More than 15,000 people depend on Bung Boraphet for their livelihoods, especially through paddy rice farming and fishing. The lake is also popular among local tourists because of its importance as a biodiversity hotspot. It provides habitat for 54 fish species (Fisheries, 2005), 252 bird species (NPWPCD, 2005) and other rare and unusual flora and fauna (ONREPP, 2002). It also becomes a home to migratory waterfowl during the dry season from November to March.

Bung Boraphet was originally a natural floodplain wetland acting as overflow storage to the Nan River during the wet season. In the 1970s, a weir was constructed and the water level was raised a further 0.20 m in 1993 to the current level of +24 m (MSL). This created the present Bung Boraphet as the largest shallow fresh water lake in central Thailand with a surface area of around 150 km^2 at the weir crest during wet seasons.

Recently Bung Boraphet has been facing problems of water clarity (low SDT and high SSC), with negative effects to the lake's ecosystem. Data collections carried out on March 31st 2009 (the dry season in Thailand) reveal that the SSC within the lake varied between 0.4 and 86 mg/l at 80 collection points with an average of around 28 mg/l, while the SDT varied between 20 and 250 cm at 80 collection points with an average value of approximately 63 cm.

Table 1
Parameters for radiance and reflectance calculations in radiometric correction.

TM Band	G ($Wm^{-2}sr^{-1}\mu m^{-1}DN^{-1}$)	B ($Wm^{-2}sr^{-1}\mu m^{-1}$)	E_0 ($Wm^{-2}\,\mu m^{-1}$)
1	0.762824	−1.5200	1957
2	1.442510	−2.8400	1826
3	1.039880	−1.1700	1554
4	0.872588	−1.5100	1036
5	0.119882	−0.3700	215.0
7	0.065294	−0.1500	80.67

3. Data collection

3.1. Satellite data

The three Landsat 5 TM images were acquired from the Geo-Informatics and Space Technology Development Agency (GISTDA). The April 13th 2008 and March 31st 2009 images were located on path 130, row 49 and the March 24th 2009 image was from path 129, row 49. There was around 13%, 10% and 20% cloud cover on the April 13th 2008, March 24th and 31st 2009 images, respectively. Conditions were cloud-free over the lake for the first image. The second and third images had 2.6% and 8.0% cloud cover over the lake, respectively. Wind speeds on these days were quite low with approximately 1.3 m/s, 1.7 m/s and 2.3 m/s, respectively. All seven TM bands were used for the analysis.

3.2. Field data collection

SDT was measured using a standard 20 cm diameter secchi disk with alternating black and white quadrants. The disk was lowered into the lake until the disk just disappeared from sight and then raised until it reappeared. The SDT value was determined as the average of both recorded depths. Water samples were collected using a Kemmerer water sampler, stored at 4 °C, then returned to the laboratory. SSC was measured by a gravimetric method using glass fiber filter paper, with the concentration calculated from differences in the weight of the filter paper before and after filtration. The dates for satellite image and ground observations of SDT and SSC were coincident on March 24th and 31st 2009. On April 15th 2008 SDT data was collected and compared with satellite image data collected on April 13th 2008 which is within the range of ±7 days which can provide reasonable results for empirical relationships between SDT, SSC and Landsat TM imagery (Kloiber et al., 2002). This is because water clarity within the lake usually does not exhibit large and rapid fluctuations during such relatively short time frames (Stadelmann et al., 2001), especially within only two days or less as the case for Bung Boraphet. The number of sampling points for SDT and SSC for each event was 80. The locations of sampling points, as shown in Fig. 2, were identified by the Global Positioning System (GPS) (Magellan Meridian Platinum), with a positional accuracy of less than 6 m.

4. Image preprocessing

4.1. Geometric correction

Geometric correction aims to remove geometric distortions introduced by a variety of factors which vary for each image acqui-

Table 2
Input parameter values for 6S model application.

Parameters	April 13th 2008	March 24th 2009	March 31st 2009
Solar zenith angle (°)	26.76	33.06	29.98
Solar azimuth angle (°)	100.73	112.36	109.37
Satellite zenith angle (°)	−6.65	7.010873	−6.105646
Aerosol model	Continental	Continental	Continental
Aerosol optical depth	0.334	0.328	0.777
Ozone (cm-atm)	0.256	0.261	0.272
Water vapor (g/cm^2)	5.337	4.402	4.65
Sensor height (km)	705	705	705
Terrain elevation (km)	0.02	0.02	0.02

Table 3
Output parameter values derived from 6S model.

Parameters	B1	B2	B3	B4	B5	B7
April 13th 2008						
Global gas transmittance (α)	0.98886	0.92479	0.93182	0.87457	0.85872	0.83938
Total scattering transmittance (β)	0.70436	0.78137	0.82986	0.87587	0.94227	0.94772
Atmospheric reflectance (ρ)	0.08445	0.04935	0.03232	0.01892	0.00417	0.00269
Spherical albedo (γ)	0.17779	0.13229	0.10305	0.07059	0.02266	0.01287
Coefficient *A* (*A*)	1.43572	1.38389	1.29319	1.30547	1.23587	1.25708
Coefficient *B* (*B*)	−0.11990	−0.06316	−0.03895	−0.21601	−0.00443	−0.00284
March 24th 2009						
Global gas transmittance (α)	0.98825	0.92445	0.93251	0.88378	0.86519	0.84625
Total scattering transmittance (β)	0.69670	0.77510	0.82471	0.87210	0.94082	0.94663
Atmospheric reflectance (ρ)	0.08400	0.04900	0.03200	0.01800	0.00400	0.00200
Spherical albedo (γ)	0.17720	0.13147	0.10221	0.06984	0.02234	0.01268
Coefficient *A* (*A*)	1.45240	1.39559	1.30031	1.29745	1.22852	1.24831
Coefficient *B* (*B*)	−0.12057	−0.06322	−0.03880	−0.02064	−0.00425	−0.00211
March 31st 2009						
Global gas transmittance (α)	0.98798	0.92270	0.93136	0.88174	0.86393	0.84522
Total scattering transmittance (β)	0.53532	0.61652	0.67475	0.74023	0.86767	0.88028
Atmospheric reflectance (ρ)	0.11400	0.07400	0.05500	0.03400	0.00900	0.00400
Spherical albedo (γ)	0.21852	0.18015	0.15290	0.11547	0.04282	0.02459
Coefficient *A* (*A*)	1.89077	1.75789	1.59125	1.53212	1.33403	1.34403
Coefficient *B* (*B*)	−0.21296	−0.12003	−0.08151	−0.04593	−0.01037	−0.00454

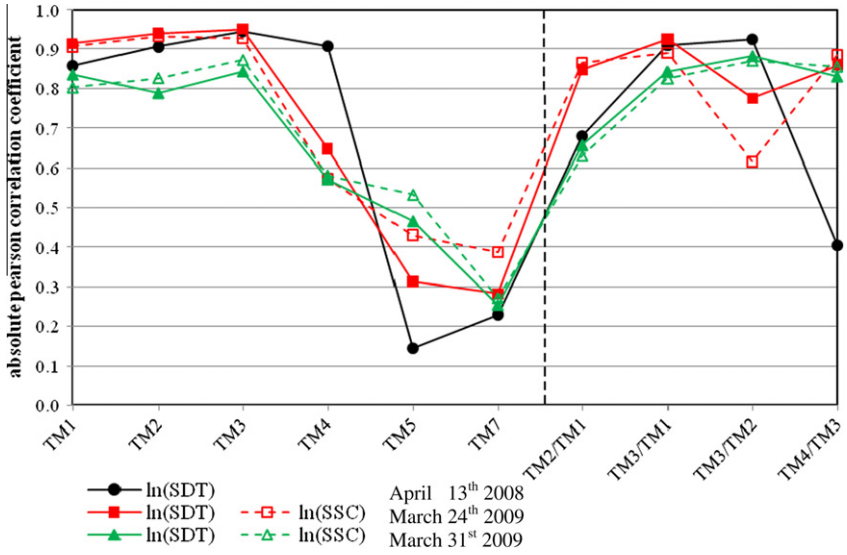

Fig. 3. Absolute Pearson correlation coefficients between ln(SDT) and ln(SSC) versus TM bands of each image.

Table 4
Step-wise multiple regressions between ln(SDT) and ln(SSC) versus TM bands of each image.

Image date	Variable	r^2	TM1	TM2	TM3	TM4	TM5	TM7
April 13th 2008	ln(SDT)	0.852			***	***	***	
March 24th 2009	ln(SDT)	0.929	*		***		**	
	ln(SSC)	0.884		**	***			*
March 31st 2009	ln(SDT)	0.854	***		***			
	ln(SSC)	0.880	***		***	***	*	

* Significance level of *p*-value < 0.10.
** Significance level of *p*-value < 0.05.
*** Significance level of *p*-value < 0.01.

sition event. Using geometric correction ensures individual picture elements (pixels) are placed in their proper planimetric map locations. Each TM image used was referenced to the Universal Transverse Mercator (UTM) Zone 47 N geographic projection using the World Geodetic System 1984 (WGS 84). The 1:50,000 scale topographic map (L7018) prepared by the Royal Thai Survey Department (RTSD) was used for image rectification. Image-to-map rectification applied for the first image (April 13th 2008), used 20 well distributed ground control points (GCPs) in the reference process. Image-to-image rectification was used for the second and third image acquired on March 24th and 31st 2009. The root mean square error (RMSE) for positional accuracy was on the order of ±0.25 pixels (6.25 m for TM data). To detect haze and cloud cover, TM band combinations 1, 6, 6 (RGB) were used. The results confirmed that the first image was cloud-free over the lake, with only minor cloud cover for the second and third

images. All image processing steps were carried out using ERDAS Imagine version 8.6. A nearest-neighbor resampling scheme was used to preserve the original brightness values of the images.

4.2. Radiometric correction

Radiometric correction transforms image data from multiple sensors and platforms into a common radiometric scale and reduces signal variations unrelated to the brightness of the imaged surface, such as spectral radiance and top-of-atmospheric reflectance. After applying radiometric correction, images taken on different dates and/or by different sensors can be directly compared. Spectral information from TM imagery is in the format of a Digital Number (DN). At-sensor spectral radiance (L) in $Wm^{-2}sr^{-1}\mu m^{-1}$ can be calculated from the remotely sensed DN values using Eq. (1).

$$L = G(\mathrm{DN}) + B \tag{1}$$

where G is the band-specific rescaling gain factor and B is the band-specific rescaling bias factor.

The characteristics of Landsat 5 have changed since it was launched, current parameter values for radiometric correction parameters as used here are presented in Table 1 (Chander and Markham, 2003; Chander et al., 2007). TM band 6, which is a thermal infrared band, is not suitable to be used for developing the relationships between in situ sampled data (SDT and SSC) versus TM data. This band measures the amount of infrared radiant flux (heat) emitted from surfaces. It is normally used in locating geothermal activity, thermal inertia mapping, vegetation classification, vegetation stress analysis, and in measuring soil moisture (Barsi et al., 2005). Therefore spectral radiance did not need to be calculated for band 6.

The spectral radiance calculated using Eq. (1) was converted to a planetary or exoatmospheric reflectance, calculated by Eq. (2), to reduce variability between scenes for better image comparison. This process can remove the cosine effect of different solar zenith angles arising from different acquisition time and can compensate for different values of the exoatmospheric solar radiances due to spectral band differences (Chander and Markham, 2003).

$$R^* = \frac{\pi d^2 L}{E_0 \cos\theta_z} \tag{2}$$

where R^* is the top of atmospheric (TOA) reflectance (unitless), d is the earth–sun distance in astronomical units, E_0 is the mean solar exoatmospheric spectral irradiance (values for different bands shown in Table 1) and θ_z is the solar zenith angle (°). The earth–sun distance (d) has a relationship to the Julian day (Dy) of the satellite data acquisition as shown in Eq. (3).

$$d = 1 - [0.01672\cos(0.9856(Dy - 4))] \tag{3}$$

4.3. Atmospheric correction

The use of satellite imagery of the Earth's surface is constrained by degradation of surface reflectance signals as a result of scattering and absorption caused by water vapor and aerosols in the atmosphere (Tanre et al., 1992). These effects depend on the wavelength of the sensor system and can vary considerably in both space and time. Aerosol scattering is stronger in the shorter solar wavelengths where the particle size is similar to the radiation wavelength. Aerosol scattering increases the apparent surface reflectance over dark surfaces. On the other hand, aerosol absorption – caused by gases such as water vapor, ozone and oxygen – reduces the apparent brightness. Atmospheric corrections to satellite data are therefore important for correcting the effects of scattering and absorption so that information from multitemporal data sets over regions with variable aerosol loading (Sharma et al., 2009) can be sensibly compared. There are two categories of atmospheric correction methods that have been developed, absolute and relative atmospheric correction (Thome et al., 1997). For the absolute correction method, the remotely sensed digital numbers are converted into surface reflectance or radiance by removing the effects of atmospheric attenuation, topographic conditions and other parameters. Different models for atmospheric correction include 6S (Second Simulation of the Satellite Signal in the Solar Spectrum), MODTRAN (Moderate Resolution Atmospheric Radiance and Transmittance Model), LOWTRAN (Low Resolution Atmospheric Transmission Model), and image-based DOS (dark object subtraction) models. Relative

Table 5
Suitable band combination for each parameter and each image.

Date	Band type	Parameter	Regression equation coefficients								r^2	SSE
			TM1	TM2	TM3	TM4	TM1/TM3	TM3/TM1	TM4/TM3	Constant		
April 13th 2008	[a]	ln(SDT)			−8.510	−6.206	1.079			3.430	0.917	0.163
	[b]	ln(SDT)			−15.879					5.373	0.892	0.183
	[c]	ln(SDT)	−16.281				3.244			2.495	0.885	0.183
	[d]	ln(SDT)	−16.281				3.244			2.495	0.885	0.191
March 24th 2009	[a]	ln(SDT)			−20.352	−2.880	0.194			5.959	0.925	0.209
	[b]	ln(SDT)			−22.01					6.111	0.926	0.207
		ln(SSC)		28.68					−0.859	−0.078	0.889	0.443
	[c]	ln(SDT)	−18.436				2.196			3.526	0.916	0.220
		ln(SSC)			39.385		0.420			−1.525	0.870	0.481
	[d]	ln(SDT)	−18.436				2.196			3.526	0.916	0.220
		ln(SSC)	39.158					2.774		−3.744	0.877	0.468
March 31st 2009	[a]	ln(SDT)			−3.786	−3.746	3.203			2.184	0.891	0.247
	[b]	ln(SDT)			−15.063					5.923	0.711	0.396
		ln(SSC)		16.006					−3.283	−3.283	0.828	0.634
	[c]	ln(SDT)	−8.232				3.758			1.596	0.893	0.243
		ln(SSC)			16.118		−3.399			4.602	0.882	0.528
	[d]	ln(SDT)	−8.232				3.758			1.596	0.893	0.243
		ln(SSC)	23.218					4.997		−5.990	0.873	0.545

[a] The most suitable band combination of the first image (April 13th 2008).
[b] The most suitable band combination of the second image (March 24th 2009).
[c] The most suitable band combination of the third image (March 31st 2009).
[d] Recommended band combination (Jie et al., 2006).

atmospheric correction aims to normalize the variation within a scene and to normalize the intensities between images of the same area acquired on different dates. The methods used in relative atmospheric correction include histogram adjustment, dark-pixel subtraction, and multi-date normalization using a regression model approach (Lu et al., 2002). Absolute atmospheric correction can remove scattering and absorption effects more accurately than the relative atmospheric correction methods. However, absolute correction requires many input parameters on in situ atmospheric conditions. Nowadays, much of the necessary information can be acquired via websites making these methods more applicable. This study used the 6S model – a physically-based absolute atmospheric correction method.

Using the 6S model, the surface reflectance free from atmospheric effect is calculated by Eq. (4) (Sharma et al., 2009).

$$R = \frac{AR^* + B}{1 + \gamma(AR^* + B)} \tag{4}$$

where R is the surface reflectance, $A = 1/\alpha\beta$, $B = -\rho/\beta$, R^* is the top of atmospheric reflectance, α is the global gas transmittance, β is the

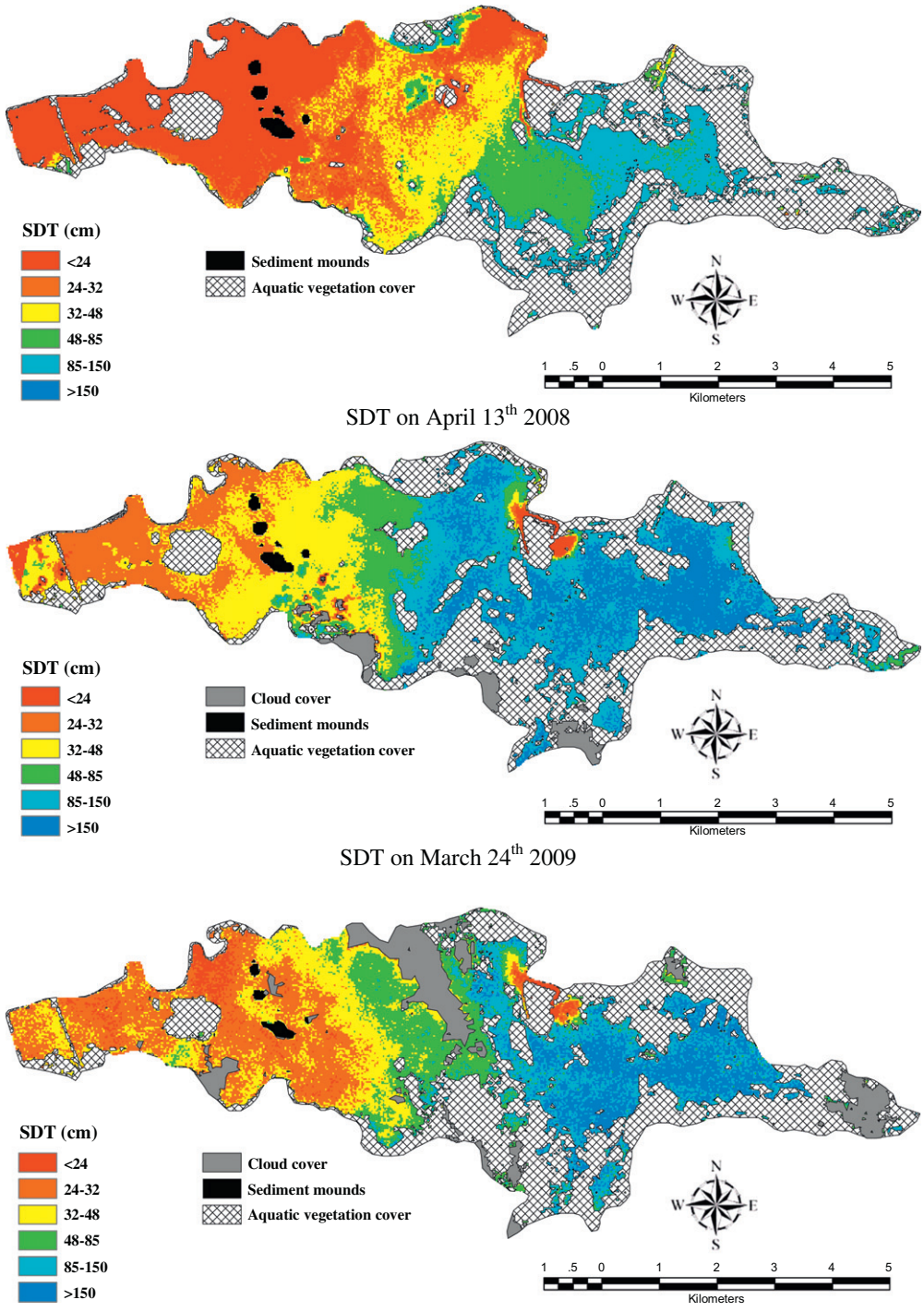

Fig. 4. Areal distributions of SDT and SSC of each image for Bung Boraphet.

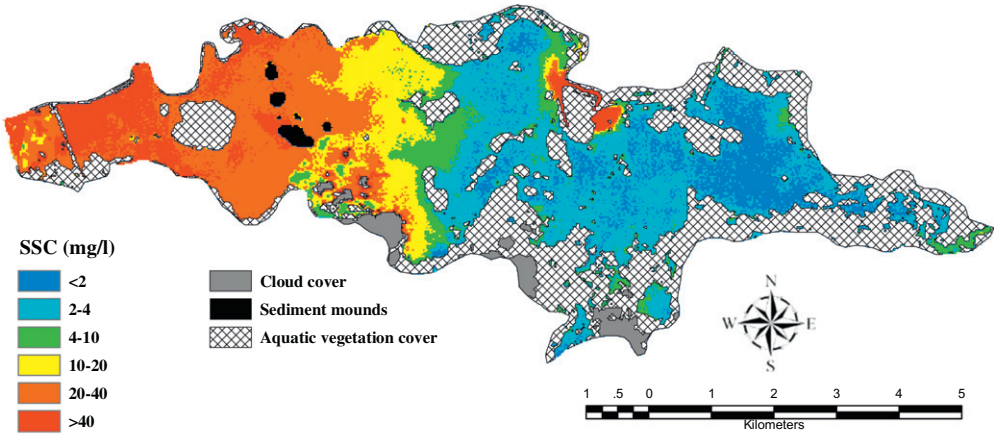

SSC on March 24th 2009

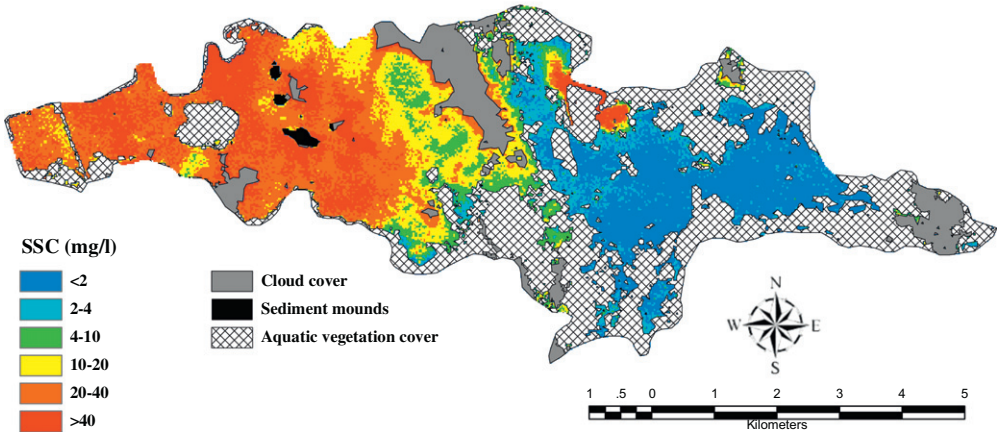

SSC on March 31st 2009

Fig. 4 (*continued*)

total scattering transmittance, ρ is the atmospheric reflectance and γ is the spherical albedo.

The parameters on the right hand side in Eq. (4) can be evaluated using the 6S model. Data needed for model application are solar zenith and azimuth angle, satellite zenith angle, date and time of image acquisition, sensor type, water vapor, ozone, aerosol optical depth (AOD), aerosol model, and target and sensor elevation. The values of solar zenith and azimuth angle, satellite zenith angle, as well as date and time of image acquisition were extracted from the header file provided together with the Landsat 5 TM data. Values of water vapor and aerosol optical depth (AOD) were retrieved from MOD08_M3.005 (MODIS Terra and Aqua Daily Global Products) through the website *http://g0dup05u.ecs.nasa.gov/Giovanni/*. Columnar ozone daily data were retrieved from L3_Ozone_OMI products available from *ftp://toms.gsfc.nasa.gov/pub/omi/data/ozone*. Table 2 shows input parameter values for the 6S model application of each TM image. Parameter values for the six bands of each TM image and TM band derived from the 6S model are presented in Table 3.

Table 6
Comparison of the retrieved values of SDT and SSC of all pixels of each image.

Image date	Parameter	Minimum	Maximum	Average	Standard deviation
April 13th 2008	SDT (cm)	11.1	186.5	36.7	21.7
March 24th 2009	SDT (cm)	7.9 (−29%)[a]	538.9 (189%)[a]	97.2 (165%)[a]	63.7 (194%)[a]
	SSC (mg/l)	0.8	236.6	10.9	17.3
March 31st 2009	SDT (cm)	13.3 (20%)[a] (68%)[b]	553.3 (197%)[a] (3%)[b]	80.9 (120%)[a] (−17%)[b]	69.4 (220%)[a] (9%)[b]
	SSC (mg/l)	0.3 (−63%)[b]	143.1 (−40%)[b]	12.8 (17%)[b]	18.6 (8%)[b]

[a] Compared percentage to the first image (April 13th 2008).
[b] Compared percentage to the second image (March 24th 2009).

5. Regression model development

5.1. Open water surface classification

There are a number of different species of emergent, floating and submergent aquatic vegetation growing in Bung Boraphet all year round. Dominant species include water lily (*Nymphaea pubescens* Willd.), sacred lotus (*Nelumbo nucifera* Gaertn.), pond weed (*Potamogeton malaianus*), water weed (*Hydrilla verticillata*), stonewort (*Chara zeylanica* Kl.ex.willd.) and bushy pond weed (*Najas graminea* Del.). It is therefore necessary to identify and exclude areas containing aquatic vegetation from the analysis. An unsupervised classification method based on a clustering algorithm called ISODATA (Iterative Self-Organizing Data Analysis Technique) with

10 clusters specified were applied to the corrected TM image data. Only field observation data points within the unvegetated water were used for formulating the empirical relationships between SDT, SSC and TM data.

5.2. Regression analyses

A Pearson correlation matrix was developed to investigate the correlations between log-transformed SDT and SSC versus TM bands of each satellite image. In general, correlation reflects the degree of linear relationship between two variables ranging from −1 and +1. A correlation of +1 means there is a perfect positive linear relationship between variables. A high level of correlation is implied by a correlation coefficient that is greater than 0.5 in absolute terms (Gupta, 1999). Fig. 3 shows that ln(SDT) and ln(SSC) were well correlated to TM1, TM2, TM3, and TM4 (the visible and near infrared regions of spectrum) but not well correlated to TM5 and TM7 (the infrared regions). TM 3 shows a slightly higher correlation to the log-transformed in situ data than other visible and near infrared bands. The results correspond to the fact that water bodies generally reflect high in the visible (band 1–3) and near infrared spectrum (band 4). In the infrared regions, water increasingly absorbs the light making it darker so these bands are useful for vegetation and soil moisture studies and for discriminating between rock and mineral types.

Several studies have proposed more complex relationships between ln(SDT), ln(SSC) and TM band ratios which possibly improve the coefficient of determination (Kloiber et al., 2002; Jie et al., 2006). This study therefore investigated the relationships between ln(SDT) and ln(SSC) versus the band ratios of TM1, TM2, TM3, and TM4, as presented in Fig. 3. The band ratio TM3/TM1 shows a uniformly high correlation to ln(SDT) and ln(SSC). TM3/TM2 also shows high correlation to the log-transformed in situ data but is less consistent. Correlations of band ratios TM2/TM1 and TM4/TM3 are also less consistent.

Backward, step-wise multiple regression analyses for 6 TM bands were performed using the thresholds for factor removal with a significance level of *p*-value more than 0.10, 0.05, and 0.01. If the *p*-value is less than the threshold, it means that the null hypothesis is rejected and the regression relationship is then reliable to be

Table 7
Comparison of TOA reflectance values of each band and image for with and without atmospheric correction.

Band	Maximum			Average			Standard deviation			Paired *t*-test		
	U	C	%	U	C	%	U	C	%	AVG	SD	*p*-value
Apirl 13th 2008												
TM1	0.349	0.357	2	0.127	0.063	−50	0.014	0.017	21	−0.065	0.005	<0.01
TM2	0.526	0.611	16	0.118	0.099	−16	0.019	0.025	32	−0.019	0.006	<0.01
TM3	0.602	0.687	14	0.105	0.096	−9	0.026	0.033	27	−0.009	0.007	<0.01
TM4	0.756	0.904	20	0.194	0.227	17	0.060	0.076	27	0.034	0.016	<0.01
TM5	0.498	0.602	21	0.154	0.184	19	0.077	0.094	22	0.031	0.017	<0.01
TM7	0.725	0.899	24	0.091	0.112	23	0.058	0.072	24	0.021	0.015	<0.01
March 24th 2009												
TM1	0.367	0.384	5	0.137	0.076	−45	0.080	0.111	39	−0.062	0.032	<0.01
TM2	0.744	0.864	16	0.128	0.112	−13	0.095	0.124	31	−0.016	0.030	<0.01
TM3	0.632	0.725	15	0.111	0.103	−7	0.095	0.118	24	−0.008	0.023	<0.01
TM4	0.794	0.943	19	0.209	0.224	7	0.134	0.167	25	0.035	0.034	<0.01
TM5	0.523	0.629	20	0.143	0.171	20	0.115	0.139	21	0.028	0.025	<0.01
TM7	0.632	0.779	23	0.089	0.109	22	0.089	0.110	24	0.020	0.022	<0.01
March 31st 2009												
TM1	0.355	0.419	18	0.170	0.106	−38	0.036	0.065	81	−0.065	0.028	<0.01
TM2	0.723	0.853	18	0.156	0.149	−4	0.054	0.083	54	−0.007	0.030	<0.01
TM3	0.614	0.788	28	0.135	0.129	−4	0.056	0.080	43	−0.005	0.025	<0.01
TM4	0.771	0.904	17	0.236	0.304	29	0.076	0.107	41	0.067	0.031	<0.01
TM5	0.508	0.648	28	0.167	0.210	26	0.082	0.107	30	0.043	0.025	<0.01
TM7	0.739	0.966	31	0.104	0.134	29	0.066	0.088	33	0.037	0.022	<0.01

Note: U = uncorrected atmospheric effect.
C = corrected atmospheric effect.

Table 8
Comparison of the retrieved values of SDT and SSC of all pixels of each image without atmospheric correction.

Image date	Parameter	Minimum	Maximum	Average	Standard deviation	Paired *t*-test *p*-value
April 13th 2008	SDT (cm)	10.9 (−2%)	162.8 (−13%)	36.8 (0.3%)	22.0 (1%)	<0.01
March 24th 2009	SDT (cm)	9.5 (20%)	404.3 (−25%)	87.3 (−10%)	62.2 (−2%)	0.10
	SSC (mg/l)	1.0 (25%)	305.8 (29%)*	11.7 (7%)	18.2 (5%)	<0.01
March 31st 2009	SDT (cm)	11.7 (−12%)	466.4 (−16%)	81.5 (1%)	65.7 (−5%)	0.05
	SSC (mg/l)	0.4 (33%)	166.5 (16%)*	12.6 (−2%)	18.9 (2%)	<0.01

Note: (−) different percentage compared to the results based on atmospheric correction.

used for prediction. Basically, *p*-value less than 0.01 is more statistical significant than *p*-value less than 0.05 and 0.10, respectively. Table 4 indicates that TM3 is the most frequently significant among all bands.

By considering the results of the Pearson correlation coefficient and step-wise regression analyses, the visible and near infrared bands as well as the band ratios TM3/TM1 and TM3/TM2 were used for investigating the most suitable relationships for estimation of SDT and SSC of each image for Bung Boraphet using multiple regression analyses. Table 5 presents regression parameters for the most suitable relationships between band combination and in situ data. As shown in Table 5, band combination relationships to SDT and SSC are unique for all images. By applying the most suitable band combination of one image to another image results in regression relationships that are reasonably well correlated as confirmed by the values of coefficient of determination (r^2) and

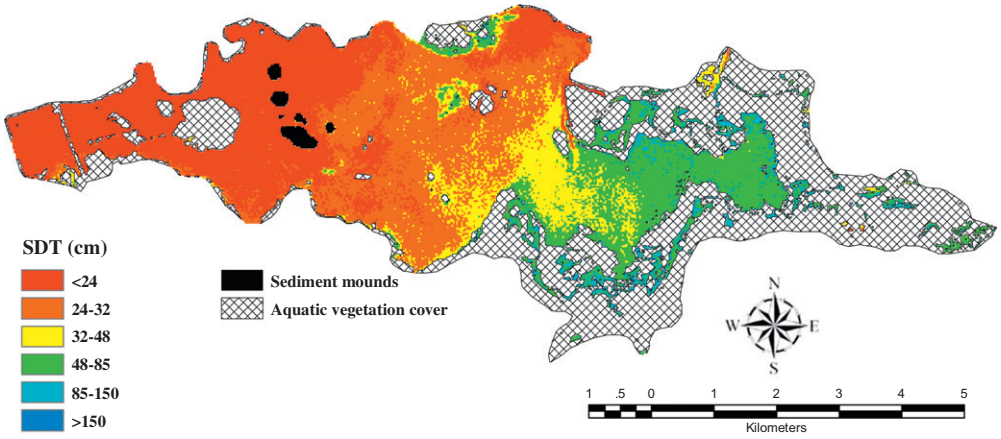

SDT on April 13th 2008

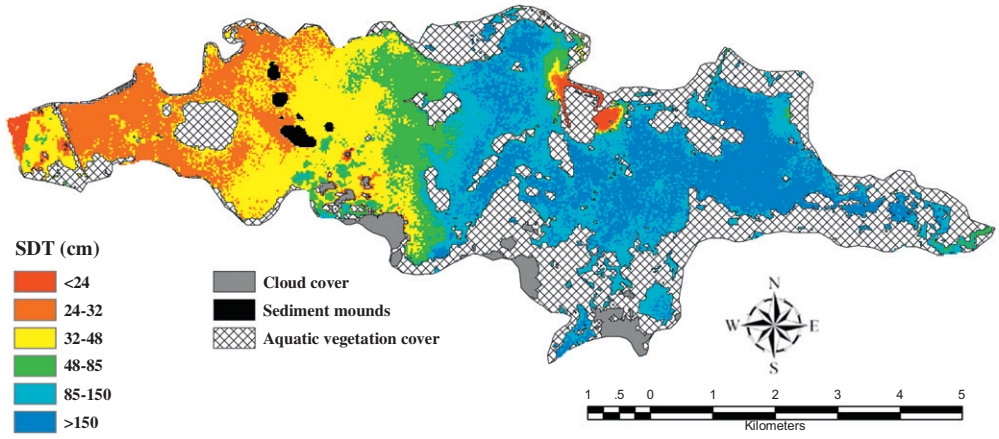

SDT on March 24th 2009

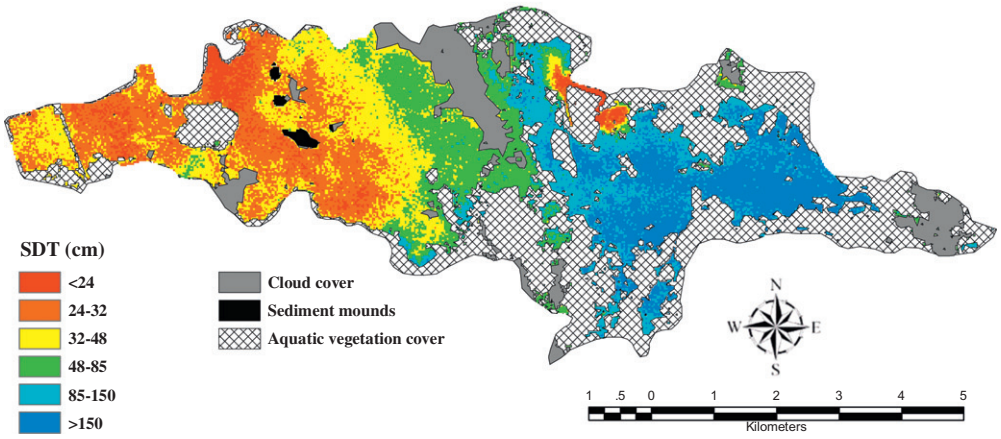

SDT on March 31st 2009

Fig. 5. Areal distributions of SDT and SSC without atmospheric correction of each image for Bung Boraphet.

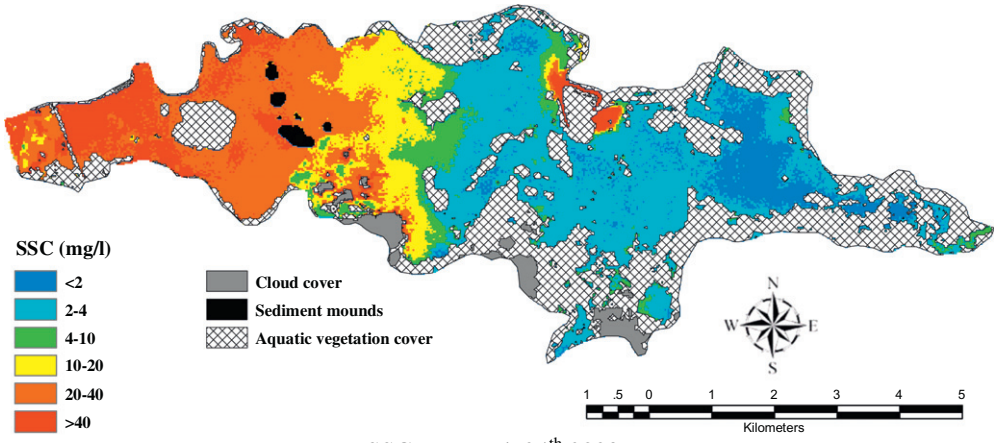

SSC on March 24th 2009

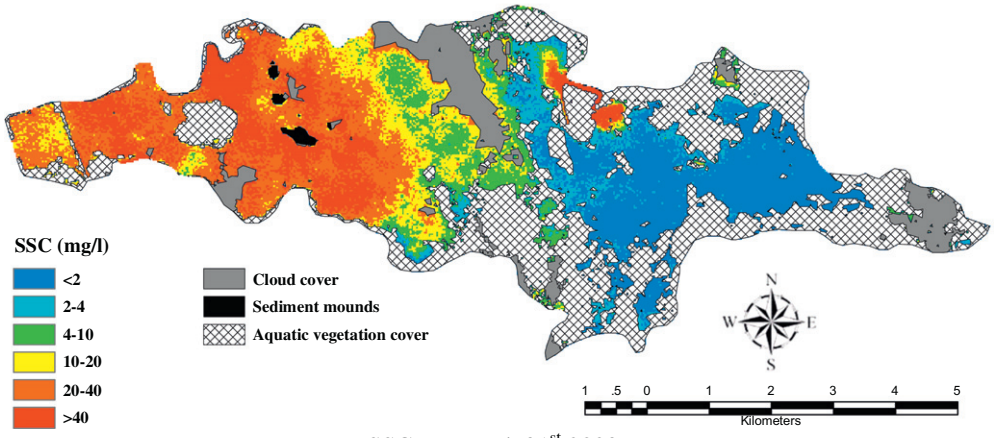

SSC on March 31st 2009

Fig. 5 (*continued*)

sum square error (SSE). It is therefore difficult to choose the most suitable band combination among these images. Band combination relationships recommended by other studies (Jie et al., 2006), as shown in Eqs. (5) and (6), were also applied for predicting SDT and SSC. The symbols *a–f* are parameters in the equations.

$$\ln(\mathrm{SDT}) = a\frac{\mathrm{TM1}}{\mathrm{TM3}} + b\mathrm{TM1} + c \tag{5}$$

$$\ln(\mathrm{SSC}) = d\frac{\mathrm{TM3}}{\mathrm{TM1}} + e\mathrm{TM1} + f \tag{6}$$

Only one relationship was found to follow the band combination recommended by Jie et al. (2006), that being the SDT relationship for the third image.

Table 5 also shows that these general band combinations, as presented in Eqs. (5) and (6), can produce acceptable values of r^2 and SSE. These band combinations were therefore applied to estimate SDT and SSC for each pixel from the three images. Lake wide SDT and SSC estimation were then ranked into 6 classes ranging from less than 24 cm to 145 cm or greater for SDT and from less than 2 mg/l to 40 mg/l or greater for SSC. Outcomes from this classification are presented in Fig. 4. SDT and SSC of each image can be roughly distinguished into 3 regions: the western region (red), the middle region (yellow to green), and the eastern region (blue). The western region shows lower SDT and higher SSC compared to other two zones. Most of this region is a fishing prohibition zone under the Fisheries Department (FD). However, a dredging operation has been ongoing in this region continuously for more than 20 years by the FD to increase lake water capacity due to high sedimentation rates within the lake. All dredged sediments are accumulated as sediment mounds which can be seen in Fig. 4. This dredging operation apparently has a high influence on water clarity, increasing SSC and reducing SDT within this zone. On the other hand, the eastern region shows lower SSC and higher SDT compared to the other two zones. There is a large amount of aquatic vegetation growing in this zone as can be seen in Fig. 4. This vegetated zone appears to enhance settling of suspended sediment and increase water clarity as indicated by the lower SSC and higher SDT values compared to other zones. The middle zone between the western and eastern zones shows medium values of SSC and SDT and appears to intermediate between them. It should be noted that the differences in extent of aquatic vegetation cover between the images on March 24th and 31st 2009 are quite significant given the relatively short temporal interval. During this period, the observed water levels changed from 23.01 to 22.94 cm. The reduction of water depth of around 7 cm during this one week was most likely responsible for the differences in extent of aquatic vegetation cover shown in Fig. 4.

Table 6 shows a summary of the estimated values of SDT and SSC at all pixels for each image. It can be seen that average SSC for the images on March 24th and 31st 2009 are not much different at around 10.9 and 12.8 mg/l, respectively, while average values of SDT are 36.7, 97.2 and 80.9 cm, respectively. The observed data has shown that water storage volumes on the April 13th 2008, March

24th and 31st 2009 were approximately 42, 76 and 72 million cubic meters, respectively, (around 24%, 43% and 41% of maximum lake storage at the weir crest). It therefore appears that SSC and SDT may be related to water storage within the lake. This is an issue that requires further study beyond the scope of this paper, as water scarcity may affect not only water available for different purposes but could play a role in reducing water clarity, with potential impacts of ecosystem stress within the lake.

5.3. Effects of atmospheric correction

Applying the 6S model for atmospheric correction to the TM bands brought about significant differences in surface reflectance to each TM band as shown in Table 7 which compares TM band values without atmospheric correction against corrected values. The corrected TOA reflectance values of the visible bands (TM1, TM2, and TM3) are generally lower than that of the uncorrected

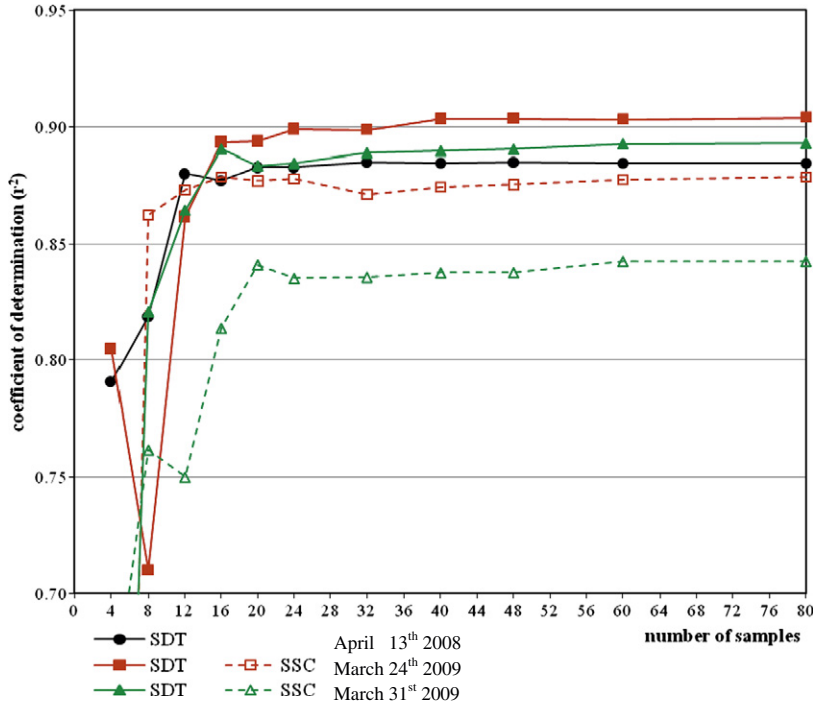

(a) Coefficient of determination (r^2)

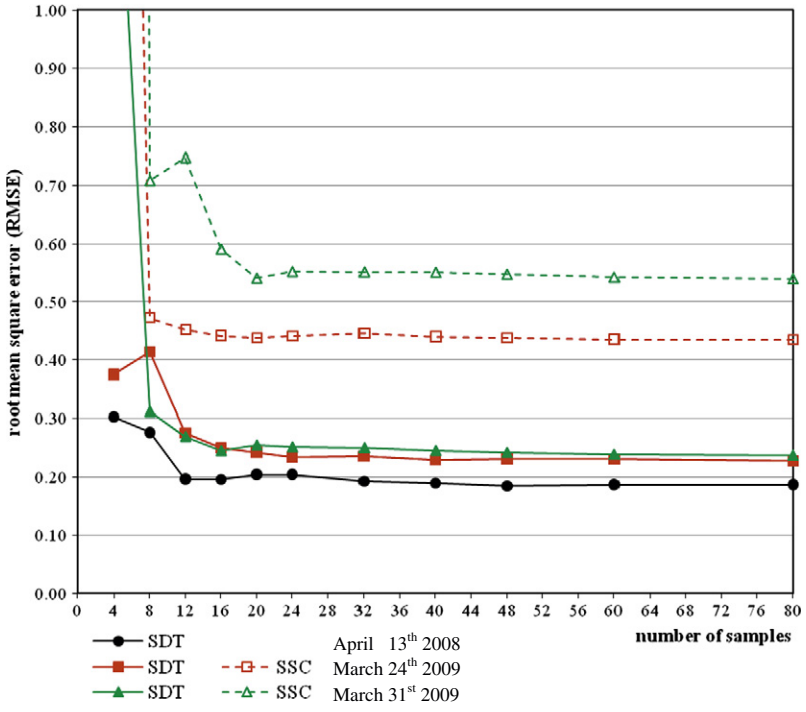

(b) Root mean square error (RMSE)

Fig. 6. Statistical values comparing observed and predicted SDT and SSC values using different number of ground sampling points of each event.

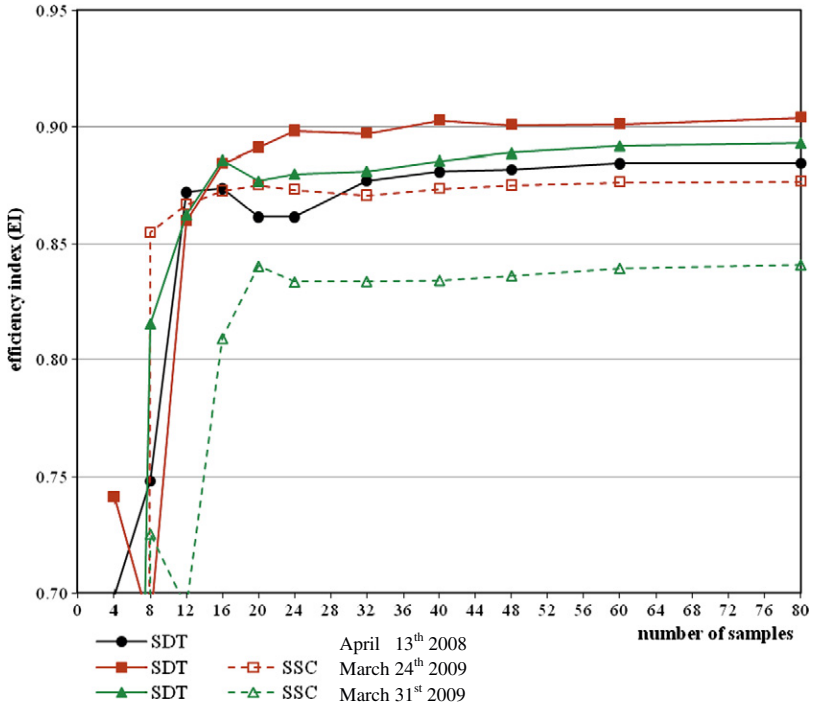

(c) Efficiency index

Fig. 6 (*continued*)

reflectance values. The averaged TOA reflectance values of these bands reduced around 50, 16, and 9% compared to the uncorrected values, respectively for the first image, around 45%, 13%, and 7%, respectively for the second image, and around 38%, 4%, and 4%, respectively for the third image. This is due to the fact that the visible bands are mainly influenced by the atmospheric rayleigh and aerosol scattering, which provide image additive effects. The 6S atmospheric correction model can remove these effects in the visible bands thereby reducing their TOA reflectance values. On the other hand, the corrected TOA reflectance values of the near infrared and infrared bands (TM4, TM5, and TM7) tend to be higher than the uncorrected reflectance values. The averaged TOA reflectance values of these bands increased around 17%, 19%, and 23% compared to the uncorrected values, respectively for the first image, around 7, 20, and 22%, respectively for the second image, and around 29, 26, and 29%, respectively for the third image. This is because the near infrared and middle infrared wavelengths are affected by atmospheric absorption while the influence of air molecules and aerosol particle scattering are negligible in these ranges. Since the 6S model can remove these effects, TOA reflectance values within these bands were then increased. Moreover, applications of the 6S model introduced significant variations in the TOA reflectance values of all TM bands. The maximum of the corrected TOA reflectance values of all bands of the three images increased within the range 2% and 31% with an average of 19% compared to the uncorrected values of each band. The standard deviation of corrected TOA reflectance values of all the bands of three images increased within the range 21% and 81% with an average of around 33% compared to the uncorrected values of each band.

For a thorough comparison of the TOA reflectance values of each band for with and without atmospheric correction, the paired *t*-test of these values at the same pixel of each image was analyzed. The average value and standard deviation of the differences between these two cases are also presented in Table 7. These different TOA reflectance values were proved to have statistical significance with the *p*-value of less than 0.01 for all bands and all images.

Table 8 presents a comparison of the estimated values of SDT and SSC for all pixels of each image without atmospheric correction. The areal distributions of SDT and SSC without atmospheric correction of each image are also shown in Fig. 5. Table 8 can be compared to Table 6 which shows the estimated values of SDT and SSC with the atmospheric correction. The percentage differences between values with and without correction are also shown in Table 8. For the first image, the average value of SDT without correction is only 0.3% higher than the corrected case. For the second and third images, the average values of SDT without correction are as much as 10% lower but only around 1% higher compared to that of with the correction, respectively. The average values of SSC without correction are as much as 7% higher but only around 2% lower compared to the corrected values, for the second and third images, respectively. The maximum and minimum values of SDT and SSC estimates with and without correction are much more different. The maximum values of SDT without correction are as much as 13%, 25%, and 16% lower compared to the corrected cases for the three images, respectively, while the maximum values of SSC without correction are as much as 29% and 16% higher compared to the corrected cases for second and third images, respectively. The minimum values of SDT without correction are 2%, and 12% lower for the first and third images, respectively, but 20% higher for the second image compared to the corrected values for the three images, respectively. The minimum values of SSC without correction are as much as 25% and 33% higher compared to the corrected values for the second and third images, respectively. It can be concluded that an application of atmospheric correction has a more significant effect on the maximum and minimum values than the effect on their average values.

The paired *t*-test of the estimated values of SDT and SSC at the same pixel for with and without atmospheric correction of each image was also compared, and the results are presented in Table 8.

Table 9
Accuracy of predicted SDT and SSC values using different number of ground sampling points.

SDT				SSC			
N	R	RMSE	EI	N	R	RMSE	EI
April 13th 2008							
80	0.885	0.187	0.885		–	–	–
60	0.885 (0.0%)	0.187 (0.0%)	0.885 (0.0%)		– –	– –	– –
48	0.885 (0.0%)	0.185 −(1.0%)	0.882 −(0.3%)		– –	– –	– –
40	0.885 (0.0%)	0.190 (1.6%)	0.881 −(0.4%)		– –	– –	– –
32	0.885 (0.0%)	0.193 (3.2%)	0.877 −(0.8%)		– –	– –	– –
24	0.883 −(0.2%)	0.205 (9.6%)	0.861 −(2.6%)		– –	– –	– –
20	0.883 −(0.2%)	0.205 (9.6%)	0.861 −(2.6%)		– –	– –	– –
16	0.877 −(0.9%)	0.195 (4.6%)	0.874 −(1.2%)		– –	– –	– –
12	0.880 −(0.5%)	0.197 (5.2%)	0.872 −(1.4%)		– –	– –	– –
8	0.819 −(7.5%)	0.276 (47.7%)	0.748 −(15.4%)		– –	– –	– –
4	0.791 −(10.6%)	0.302 (61.7%)	0.699 −(21.0%)		– –	– –	– –
March 24th 2009							
80	0.904	0.229	0.904	80	0.879	0.435	0.877
60	0.903 −(0.08%)	0.232 (1.39%)	0.901 −(0.30%)	60	0.877 −(0.14%)	0.436 (0.15%)	0.876 −(0.04%)
48	0.903 −(0.04%)	0.232 (1.58%)	0.901 −(0.34%)	48	0.875 −(0.38%)	0.438 (0.68%)	0.875 −(0.19%)
40	0.903 −(0.06%)	0.230 (0.61%)	0.903 −(0.13%)	40	0.874 −(0.50%)	0.440 (1.22%)	0.874 −(0.34%)
32	0.899 −(0.56%)	0.236 (3.38%)	0.897 −(0.73%)	32	0.871 −(0.85%)	0.446 (2.43%)	0.871 −(0.69%)
24	0.899 −(0.54%)	0.235 (2.91%)	0.898 −(0.63%)	24	0.878 −(0.08%)	0.441 (1.40%)	0.873 −(0.40%)
20	0.894 −(1.12%)	0.243 (6.45%)	0.891 −(1.42%)	20	0.877 −(0.20%)	0.438 (0.64%)	0.875 −(0.18%)
16	0.893 −(1.17%)	0.251 (9.61%)	0.885 −(2.14%)	16	0.879 (0.00%)	0.442 (1.63%)	0.873 −(0.46%)
12	0.862 −(4.67%)	0.276 (20.76%)	0.860 −(4.87%)	12	0.873 −(0.63%)	0.452 (3.97%)	0.867 −(1.14%)
8	0.710 −(21.45%)	0.413 (80.83%)	0.686 −(24.14%)	8	0.862 −(1.86%)	0.472 (8.56%)	0.855 −(2.51%)
4	0.805 −(10.96%)	0.375 (63.93%)	0.742 −(17.95%)	4	0.246 −(72.06%)	3.274 (652.23%)	−5.972 −(781.18%)
March 31st 2009							
80	0.893	0.238	0.893	80	0.842	0.539	0.841
60	0.893 −(0.02%)	0.239 (0.57%)	0.892 −(0.14%)	60	0.842 (0.00%)	0.542 (0.47%)	0.839 −(0.18%)
48	0.890 −(0.28%)	0.242 (1.93%)	0.889 −(0.47%)	48	0.837 −(0.57%)	0.547 (1.43%)	0.836 −(0.55%)
40	0.890 −(0.35%)	0.246 (3.39%)	0.885 −(0.83%)	40	0.837 −(0.59%)	0.550 (2.07%)	0.834 −(0.79%)
32	0.889 −(0.45%)	0.250 (5.33%)	0.881 −(1.31%)	32	0.835 −(0.81%)	0.551 (2.20%)	0.834 −(0.84%)
24	0.885 −(0.93%)	0.252 (5.87%)	0.880 −(1.45%)	24	0.835 −(0.87%)	0.552 (2.28%)	0.833 −(0.87%)
20	0.883 −(1.06%)	0.255 (7.24%)	0.877 −(1.80%)	20	0.841 −(0.18%)	0.540 (0.18%)	0.840 −(0.07%)

Table 9 (*continued*)

SDT				SSC			
N	R	RMSE	EI	N	R	RMSE	EI
16	0.890 −(0.27%)	0.246 (3.29%)	0.886 −(0.80%)	16	0.814 −(3.42%)	0.590 (9.45%)	0.809 −(3.75%)
12	0.864 −(3.20%)	0.270 (13.37%)	0.862 −(3.42%)	12	0.750 −(10.97%)	0.748 (38.66%)	0.694 −(17.48%)
8	0.821 −(8.09%)	0.312 (31.24%)	0.815 −(8.67%)	8	0.762 −(9.59%)	0.708 (31.29%)	0.725 −(13.72%)
4	0.381 −(57.32%)	1.450 (509.82%)	−2.985 −(434.28%)	4	0.647 −(23.16%)	15.358 (2747.75%)	−128.203 −(15349.87%)

n = number of ground sampling points.
(%) Different percentage compared to the case of using the maximum number of ground sampling points of each parameter and each image.

The table shows that these different values of SDT and SSC between these two cases were proved to have statistical significance. The *p*-value for SSC was less than 0.01 for all images, while the *p*-value for SDT was less than 0.01, 0.05, and 0.10 for the first, the third, and the second image, respectively.

5.4. Effect of the number of ground sampling points on the accuracy of predicted SDT and SSC values

Ground observation data of SDT and SSC are critical in developing empirical relationships between SDT, SSC and Landsat TM images in a lake. Ground data collection is however time consuming and quite expensive, especially the SSC laboratory cost. In this section, the minimum number of ground observation points of SDT and SSC necessary for creating reliable relationships were evaluated. The random number table available in "a Million Random Digits with 100,000 Normal Deviates" (RAND, 2001) was applied to eliminate some of the sampling points in an unbiased manner. Trialed random subsampling points were 80, 60, 48, 40, 32, 24, 20, 16, 12, 8, and 4, which represent 100–5% of the overall 80 sampling points, respectively. The TM values at these points were then subjected to regression against SDT and SSC as shown in Fig. 6 and Table 9. Empirical relationships using these ground data subsets and the TM images were calculated and were then applied to estimate the values of SDT and SSC of each image at all original sampling points.

Observed and predicted SDT and SSC values at each sampling point for each image were compared for their accuracy and the results are summarized in Table 9 and in Fig. 6. Table 9 and Fig. 6 show that if the number of points is reduced to below 20 points, significantly lower coefficient of determination (r^2) and efficiency index (EI), and higher root mean square error (RMSE) are obtained.

To make sure of our conclusion, the effects of sampling points on percent change of average and coefficient of variation of SDT and SSC compared to the maximum sampling points were plotted as shown in Fig. 7 and Table 10. Both Fig. 7a, the percent change of averaged SDT and SSC, and Fig. 7b, the percent change of coefficient of variance for SDT and SSC, show that the number of sampling points does not have much effect on the average and coefficient of variation of SDT and SSC compared to the maximum sampling points until the number of points is lower than 32. Once the numbers of sampling points is lower than 32, the percent change of average and coefficient of variation of SDT and SSC tend to significantly divert from the zero percent line. Less sampling points tend to have more effect on increasing the percent change of average and coefficient of variation of SDT and SSC.

It can be concluded that with a random sampling pattern across the lake, the number of ground observation points of SDT and SSC should not be less than 32 to yield reliable predictions for SDT and SSC within the lake. This gives a good tradeoff between the accuracy of SDT and SSC predictions and the sampling cost. The locations of the 32 sampling points chosen are shown in Fig. 8.

6. Conclusion

This study of the spatial distribution of SDT and SSC in Bung Boraphet has been undertaken to assess suspended sediment concentration and transparency. Three Landsat 5 TM images and ground observation data of SDT and SSC, which are nearly contemporaneous and contemporaneous with the image acquisition time, were collected to generate empirical relationships for each parameter. SDT and SSC values distributed across the lake were then determined. To be noted that a longer time window would possibly affect the reliability of generated empirical relationships. The contemporaneous between satellite image and ground sampling points are recommended, especially for the ground sampling parameter values that can vary significantly in a relatively short time frame.

Prior to generating empirical relationships, the geometric correction, radiometric correction, as well as atmospheric correction to these TM data were implemented during the image preprocessing step. In the regression model development processes, ground observation data points within open water areas were used to develop the relationships.

Pearson correlation coefficients and backward, step-wise multiple regression analyses were used to investigate the correlations between log-transformed SDT and SSC versus TM bands and the band ratios of each satellite image. The results revealed that the visible and near infrared band and the band ratios TM3/TM1 and TM3/TM2 were suitable to be used for investigating the most suitable relationships. However the most suitable band combination for both SDT and SSC of these three images are different. The reliable common band combinations TM1/TM3 and TM1 were therefore applied to estimate ln(SDT), and TM3/TM1 and TM1 to estimate ln(SSC). These empirical relationships yield reliable estimates for spatial distributions of SDT and SSC within the lake for each satellite image.

Regarding the first objective of this study on the importance of atmospheric corrections, the application of the 6S model has proved to have the effect on the average values of SDT and SSC, and especially on their maximum and minimum values, for the series of three events from 2008 to 2009 in Bung Boraphet. It was confirmed by the paired *t*-test, which showed statistical significance of the different SDT and SSC values between with and without atmospheric correction for those three events. Atmospheric correction is therefore suggested to be applied to reduce the effects of scattering and absorption caused by water vapor and aerosols in the atmosphere. However, the 6S model is one of the models for remote sensing image atmosphere correction, it is recommended

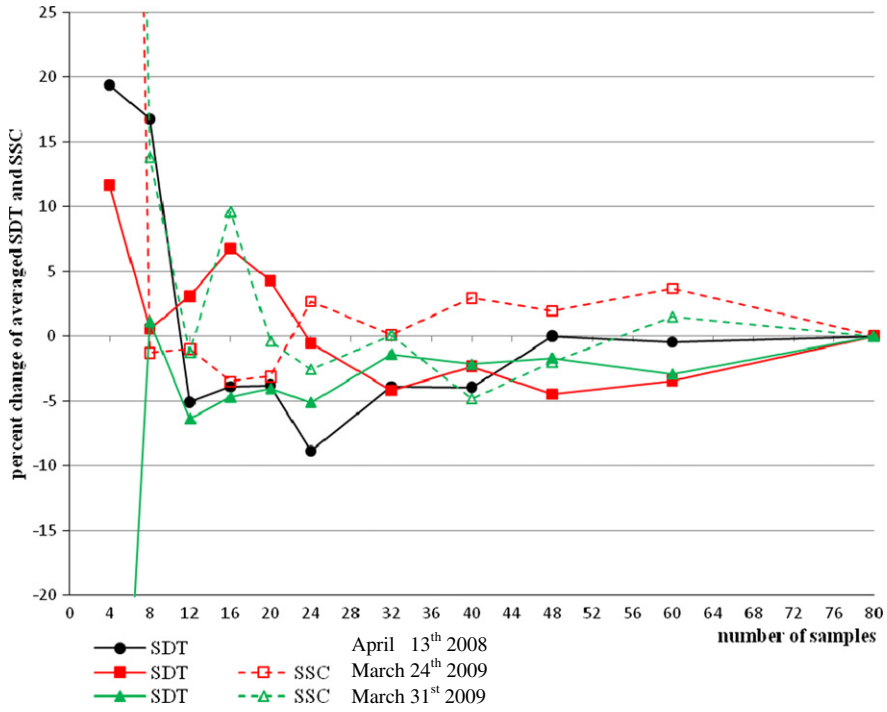

(a) Percent change of averaged SDT and SSC

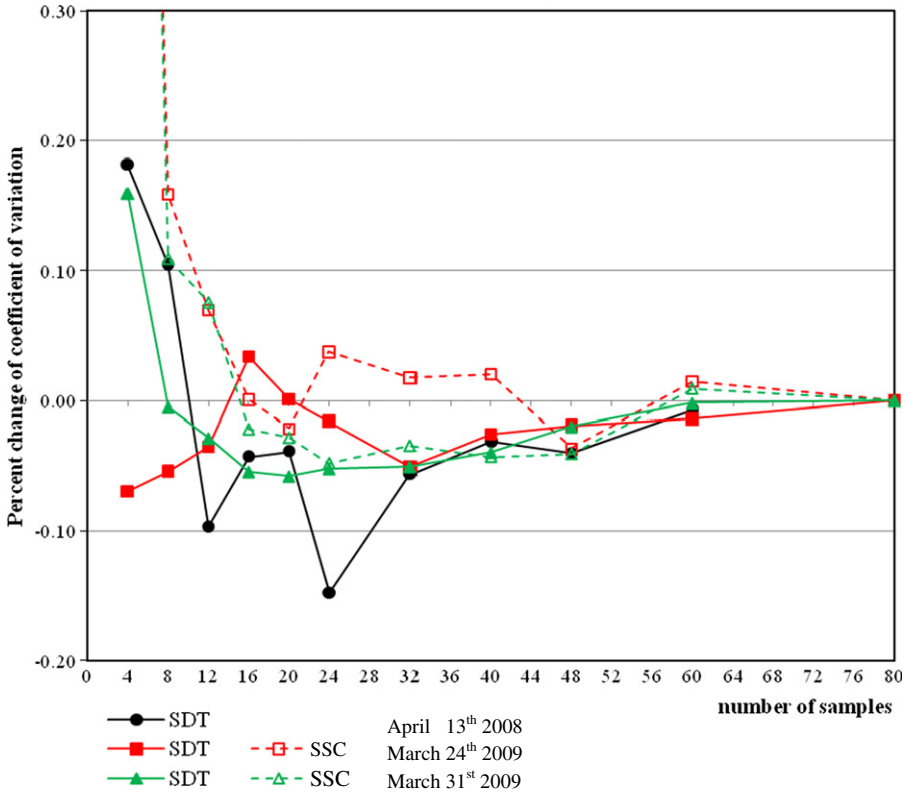

(b) Percent change of coefficient of variation (SD/average) of SDT and SSC

Fig. 7. Effects of sampling points on percent change of average and coefficient of variation of SDT and SSC compared to the maximum sampling points.

to apply other models (especially models of other types) to do some comparison works.

Regarding the second objective on the importance of the number of sampling point, the minimum number of ground sampling points of SDT and SSC necessary for creating the reliable relationships were investigated. By reducing the number of observations of SDT and SSC to be 32 points across the lake (less than half of the original 80 points), it would still be possible to obtain a reliable relationship for the estimation of SDT and SSC values distributed within the lake. By comparing the number of sampling points and surface areas of the open water, it is approximately one sampling point per 0.85 km^2 of the surface area. Since these sampling points

Table 10
Average and coefficient of variation of retrieved SDT and SSC values.

Number	April 13th 2008		March 24th 2009				March 31st 2009			
	SDT		SDT		SSC		SDT		SSC	
	AVG	SD/avg	AVG	SD/avg	AVG	SD/avg	AVG	SD/avg	AVG	SD/avg
79	36.7	0.59	97.24	0.65	10.88	1.59	80.98	0.86	12.78	1.45
60	36.53 −(0.50%)	0.59 −(0.50%)	93.91 −(0.50%)	0.65 −(0.50%)	11.28 −(0.50%)	1.61 −(0.50%)	78.61 −(0.50%)	0.86 −(0.50%)	12.97 −(0.50%)	1.47 −(0.50%)
48	36.78 −(0.20%)	0.57 −(3.98%)	92.9 −(4.46%)	0.64 −(1.85%)	11.09 −(1.93%)	1.53 −(3.60%)	79.62 −(1.68%)	0.84 −(1.96%)	12.52 −(2.03%)	1.39 −(4.03%)
40	35.25 −(4.00%)	0.57 −(3.07%)	94.98 −(2.32%)	0.64 −(2.54%)	11.2 −(2.94%)	1.62 −(2.03%)	79.23 −(2.16%)	0.82 −(3.92%)	12.16 −(4.85%)	1.39 −(4.24%)
32	35.27 −(3.90%)	0.56 −(5.61%)	93.19 −(4.16%)	0.62 −(5.01%)	10.89 −(0.09%)	1.62 −(1.76%)	79.87 −(1.37%)	0.81 −(5.00%)	12.79 −(0.08%)	1.4 −(3.42%)
24	33.45 −(8.90%)	0.5 −(14.76%)	96.73 −(0.52%)	0.64 −(1.53%)	11.17 −(2.67%)	1.65 −(3.77%)	76.84 −(5.11%)	0.81 −(5.17%)	12.45 −(2.58%)	1.38 −(4.76%)
20	35.31 −(3.80%)	0.57 −(3.86%)	101.39 −(4.27%)	0.66 −(0.12%)	10.54 −(3.13%)	1.56 −(2.09%)	77.7 −(4.05%)	0.81 −(5.75%)	12.73 −(0.39%)	1.41 −(2.80%)
16	35.26 −(3.90%)	0.57 −(4.25%)	103.83 −(6.78%)	0.68 −(3.39%)	10.5 −(3.49%)	1.59 −(0.08%)	77.16 −(4.72%)	0.81 −(5.40%)	14.01 −(9.62%)	1.42 −(2.14%)
12	34.83 −(5.10%)	0.54 −(9.66%)	100.24 −(3.09%)	0.63 −(3.48%)	10.77 −(1.01%)	1.7 −(6.98%)	75.82 −(6.37%)	0.83 −(2.83%)	12.62 −(1.25%)	1.56 −(7.60%)
8	42.85 −(16.80%)	0.65 −(10.51%)	97.8 −(0.58%)	0.62 −(5.37%)	10.74 −(1.29%)	1.84 −(15.89%)	81.91 −(1.15%)	0.85 −(0.49%)	14.55 −(13.85%)	1.61 −(10.98%)
4	43.81 −(19.40%)	0.7 −(18.18%)	108.57 −(11.65%)	0.61 −(6.92%)	29.11 −(167.56%)	3.59 −(125.98%)	36.98 −(54.33%)	0.99 −(15.96%)	33.5 −(162.13%)	3.39 −(133.58%)

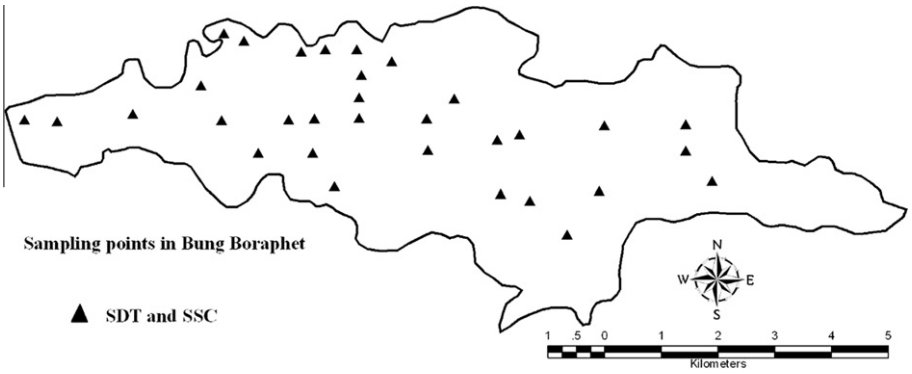

Fig. 8. Locations of 32 sampling locations of SDT and SSC within the lake.

were selected based on random method, the future operational monitoring locations of SDT and SSC in Bung Boraphet for these 32 sampling points will be selected to be evenly distributed across the open water surface for a particular event.

Acknowledgements

The authors gratefully acknowledge the Thailand Research Fund through the Royal Golden Jubilee Ph.D. program (Grant No. PhD/0077/2551) and the Kasetsart University Research and Development Institute for financially supporting this research. We also would like to thank Dr. Michael Waters for editing the manuscript.

References

Barsi, J.A., Schott, J.R., Palluconi, F.D., Hook, S.J., 2005. Validation of a web-based atmospheric correction tool for single thermal band instruments. In: Proceedings of Earth Observing Systems X, SPIE, Bellingham, WA.

Brown, D., Warwick, R., Skaggs, R., 1977. Reconnaissance Analysis of Lake Condition in East – Central Minnesota. Report No. 5022. Minnesota Land Management Information System, Center for Urban and Regional Affairs. University of Minnesota, Minneapolis, MN, 19 pp.

Chander, G., Markham, B., 2003. Revised landsat-5 TM radiometric calibration procedures and postcalibration dynamic ranges. IEEE Transactions on Geoscience and Remote Sensing 41 (11), 2674–2677.

Chander, G., Markham, B., Barsi, J.A., 2007. Revised landsat-5 thematic mapper radiometric calibration. IEEE Geoscience and Remote Sensing Letters 4 (3), 490–494.

Fisheries, 2005. The Survey of Fish Population in Bung Boraphet. Bangkok, Thailand. Nakorn Sawan Inland Fisheries Development Center, Fisheries Department.

Giardino, C., Pepe, M., Brivio, P.A., Ghezzi, P., Zilioli, E., 2001. Detecting chlorophyll, Secchi disk depth and surface temperature in a sub-alpine lake using Landsat imagery. Science of the Total Environment 268 (1–3), 19–29.

Gupta, V., 1999. SPSS for Beginners. VJbooks Inc., USA.

Heiskary, S.A., Lindbloom, J., Wilson, C.B., 1994. Detecting water quality trends with citizen volunteer data. Lake and Reservoir Management 9, 4–9.

Jie, G., Yuchun, W., Jiazhu, H., 2006. A model for the retrieval of suspended sediment concentrations in Taihu Lake from TM images. Journal of Geographical Sciences 16 (4), 458–464.

Klemas, V., Bartlett, D., Philpot, W., 1974. Coastal and estuarine studies with ERTS-1 and Skylab. Remote Sensing of Environment 3 (3), 153–174.

Kloiber, S.M., Brezonik, P.L., Olmanson, L.G., Bauer, M.E., 2002. A procedure for regional lake water clarity assessment using Landsat multispectral data. Remote Sensing of Environment 82, 38–47.

Lathrop, R.G., Lillesand, T.M., 1986. Utility of thematic Mapper data to assess water quality in southern Green Bay and west-central Lake Michigan. Photogrammetric Engineering and Remote Sensing 52, 671–680.

Lu, D., Mausel, P., Brondizio, E., Moran, E., 2002. Assessment of atmospheric correction methods for Landsat TM data applicable to Amazon basin LBA research. International Journal of Remote Sensing 23, 2651–2671.

Liu, Y., Islam, M.A., Gao, J., 2003. Quantification of shallow water quality parameters by means of remote sensing. Progress in Physical Geography 27 (1), 24–43.

NPWPCD, 2005. Survey of Wildlife in Bung Boraphet. Annual Research Report. Bung Boraphet Wildlife Research Center, National Park, Wildlife and Plants Conservation Department.

Olmanson, L.G., Bauer, M.E., Brezonik, P.L., 2008. A 20-year Landsat water clarity census of Minnesota's 10,000 lakes. Remote Sensing of Environment 112, 4086–4097.

ONREPP, 2002. The Biodiversity in Bung Boraphet Wetland. Bangkok, Thailand, Office of Natural Resources and Environmental Policy and Planning.

Ostlund, C., Flink, P., Strombeck, N., Piersonb, D., Lindell, T., 2001. Mapping of the water quality of Lake Erken, Sweden, from imaging spectrometry and Landsat Thematic Mapper. The Science of the Total Environment 268, 139–154.

Oyama, Y., Matsushita, B., Fukushima, T., Matsushige, K., Imai, A., 2009. Application of spectral decomposition algorithm for mapping water quality in a turbid lake (Lake Kasumigaura, Japan) from Landsat TM data. IRPRS Journal of Photogrammetry and Remote Sensing 64, 73–85.

Pattiaratchi, C., Lavery, P., Wyllie, A., Hick, P., 1974. Estimates of water quality in coastal waters using multi-date Landsat Thematic Mapper data. International Journal of Remote Sensing 15, 1571–1584.

RAND, 2001. A Million Random Digits with 100,000 Normal Deviate 1955. Free Press, Santamonica, CA, USA.

Sharma, A.R., Badarinath, K.V.S., Roy, P.S., 2009. Comparison of ground reflectance measurement with satellite derived atmospherically corrected reflectance. A case study over semi-arid landscape. Advances in Space Research 43, 56–64.

Stadelmann, T.H., Brezonik, P.L., Kloiber, S., 2001. Seasonal patterns of chlorophyll a and Secchi disk transparency in lakes of east-central minnesota: implications for design of ground-and satellite-based monitoring programs. Lake and Reservoir Management 17 (4), 299–314.

Stroeve, J., Nolin, A., Steffen, K., 1997. Comparison of AVHRR-derived and in situ surface albedo over the Greenland ice sheet. Remote Sensing of Environment 62, 262–276.

Tanre, D., Holben, B.N., Kaufman, Y.J., 1992. Atmospheric correction against algorithm for NOAA-AVHRR products: theory and application. IEEE Transactions on Geoscience and Remote Sensing 30 (2), 231–248.

Thome, K., Markham, B., Barker, J., Slater, P., Biggar, S., 1997. Radiometric calibration of Landsat. Photogrammetric Engineering and Remote Sensing 63, 835–858.

Zhao, W., Tamura, M., Takahashi, H., 2001. Atmospheric and spectral corrections for estimating surface albedo from satellite data using 6S code. Remote Sensing of Environment 76, 202–212.